High-Temperature Rate Constants for $CH_3OH + Kr \rightarrow$ Products, $OH + CH_3OH \rightarrow$ Products, $OH + (CH_3)_2CO \rightarrow CH_2COCH_3 + H_2O$, and $OH + CH_3 \rightarrow CH_2 + H_2O$†

N. K. Srinivasan, M.-C. Su,‡ and J. V. Michael*

Chemistry Division, Argonne National Laboratory, Argonne, Illinois 60439

Received: November 7, 2006; In Final Form: December 12, 2006

The reflected shock tube technique with multipass absorption spectrometric detection of OH radicals at 308 nm (corresponding to a total path length of ∼4.9 m) has been used to study the dissociation of methanol between 1591 and 2865 K. Rate constants for two product channels [$CH_3OH + Kr \rightarrow CH_3 + OH + Kr$ (1) and $CH_3OH + Kr \rightarrow {}^1CH_2 + H_2O + Kr$ (2)] were determined. During the course of the study, it was necessary to determine several other rate constants that contributed to the profile fits. These include $OH + CH_3OH \rightarrow$ products, $OH + (CH_3)_2CO \rightarrow CH_2COCH_3 + H_2O$, and $OH + CH_3 \rightarrow {}^{1,3}CH_2 + H_2O$. The derived expressions, in units of cm^3 molecule^{-1} s,$^{-1}$ are $k_1 = 9.33 \times 10^{-9} \exp(-30857\ K/T)$ for 1591−2287 K, $k_2 = 3.27 \times 10^{-10} \exp(-25946\ K/T)$ for 1734−2287 K, $k_{OH+CH_3OH} = 2.96 \times 10^{-16} T^{1.4434} \exp(-57\ K/T)$ for 210−1710 K, $k_{OH+(CH_3)_2CO} = (7.3 \pm 0.7) \times 10^{-12}$ for 1178−1299 K and $k_{OH+CH_3} = (1.3 \pm 0.2) \times 10^{-11}$ for 1000−1200 K. With these values along with other well-established rate constants, a mechanism was used to obtain profile fits that agreed with experiment to within $<\pm 10\%$. The values obtained for reactions 1 and 2 are compared with earlier determinations and also with new theoretical calculations that are presented in the preceding article in this issue. These new calculations are in good agreement with the present data for both (1) and (2) and also for $OH + CH_3 \rightarrow$ products.

Introduction

The thermal decomposition of methanol has been extensively investigated by several workers over a span of 30 years[1] because CH_3OH is an important alternative fuel in combustion. As pointed out in these earlier studies, there are at least six possible decomposition channels,

$$CH_3OH \rightarrow CH_3 + OH \quad (1)$$

$$\rightarrow {}^1CH_2 + H_2O \quad (2)$$

$$\rightarrow CH_2OH/CH_3O + H \quad (3)$$

$$\rightarrow CH_2O + H_2 \quad (4)$$

$$\rightarrow cis\text{-}HCOH + H_2 \quad (5)$$

$$\rightarrow trans\text{-}HCOH + H_2 \quad (6)$$

The most recent experimental measurements on methanol decomposition were conducted in this laboratory[2] using a Fabry−Perot design multipass OH absorption cell coupled to the shock tube. The k_{total} values agreed well with the experimental measurements of Cribb et al.[3] and with a majority of the other studies.[1] Hence, there is good agreement on the overall second-order rate constants, but there are discrepancies in the predicted branching ratios for the various channels as discussed by Xia et al.[4] who carried out extensive theoretical rate constant calculations. In their work, their k_{total} values underestimated the experimental results by at least an order of magnitude. However, over the entire pressure and temperature ranges, these calculations suggested significance for some of the channels (1)−(6). The earlier results from this laboratory[2] conclude that reaction (1) is the dominant process.

We earlier described a long absorption path multipass optical system for OH-radical detection in the reflected shock regime[5] and used it to measure other high-temperature rate constants.[6−8] In this work we have increased the path length for absorption by using 56 optical passes giving a total path length of 4.897 m. Hence, the sensitivity for OH-radical detection is about 5 times greater than in the earlier studies.[2,5] With enhanced OH-radical sensitivity and better signal-to-noise, CH_3OH dissociation could be accurately studied over a wider *T*-range (1591−2865 K), allowing measurements of product branching ratios. This supplies the motivation for the present study.

Experimental Section

The present experiments were performed with the shock tube technique using OH-radical electronic absorption detection. The method and the apparatus currently being used have been previously described,[9,10] and only a brief description of the experiment will be presented here.

Apparatus and Method. The shock tube is constructed from 304 stainless steel in three sections. The first 10.2 cm-o.d. cylindrical section is separated from the He driver chamber by a 4 mil unscored 1100-H18 aluminum diaphragm. A 0.25 m transition section then connects the first and third sections. The third section is of rounded corner (radius, 1.71 cm) square design and is fabricated from flat stock (3 mm) with a mirror finish. Two flat fused silica windows (3.81 cm) with broadband antireflection (BB AR) coating for UV light are mounted on

† Part of the special issue "James A. Miller Festschrift".

* To whom correspondence should be addressed. Address: D-193, Bldg. 200, Argonne National Laboratory, Argonne, IL 60439. Phone: (630) 252-3171. Fax: (630) 252-4470. E-mail: jmichael@anl.gov.

‡ Special Term Appointment, Argonne. Permanent address: Department of Chemistry, Sonoma State University, 1801 E. Cotati Ave., Rohnert Park, CA 94928.

10.1021/jp0673516 CCC: $37.00
Published on Web 03/16/2007

the tube across from one another at a distance of 6 cm from the end plate. The path length between windows is 8.745 cm. The incident shock velocity is measured with eight fast pressure transducers (PCB Piezotronics, Inc., Model 113A21) mounted along the third portion of the shock tube, and temperature and density in the reflected shock wave regime are calculated from this velocity and include corrections for boundary layer perturbations.[11−13] The tube is routinely pumped between experiments to $<10^{-8}$ Torr by an Edwards Vacuum Products Model CR100P packaged pumping system. A 4094C Nicolet digital oscilloscope was used to record both the velocity and absorption signals.

The optical configuration consists of an OH resonance lamp, multipass reflectors, an interference filter at 308 nm, and a photomultiplier tube (1P28) all mounted external to the shock tube as described previously.[5−8,14] With this new configuration, a total path length of 4.897 m was obtainable thereby amplifying the measured absorbances by 56.

Gases. High purity He (99.995%), used as the driver gas, was from AGA Gases. Scientific grade Kr (99.999%), the diluent gas in reactant mixtures, was from Spectra Gases, Inc. The ~10 ppm impurities (N_2 2 ppm, O_2 0.5 ppm, Ar 2 ppm, CO_2 0.5 ppm, H_2 0.5 ppm, CH_4 0.5 ppm, H_2O 0.5 ppm, Xe 5 ppm, and CF_4 0.5 ppm) all are either inert or are in sufficiently low concentration so as to not perturb OH-radical profiles. Distilled water, evaporated at 1 atm into ultrahigh purity grade Ar (99.999%) from AGA Gases, was used at ~25 Torr pressure in the resonance lamp. CH_3I (99.5%) from Sigma Aldrich Chemical Co. Inc., and CH_3OH (>99.0%) and acetone (>99.0%) from Chemika Fluka, were all further purified by bulb-to-bulb distillations with the middle thirds being retained. T-HYDRO *tert*-butyl hyroperoxide (70% tBH by weight water solution; i.e., 32 mol % tBH and 68 mol % H_2O) was obtained from Aldrich Chemical Co. Inc. Test gas mixtures were accurately prepared from pressure measurements using a Baratron capacitance manometer and were stored in an all glass vacuum line. In the tBH experiments, 0.45 cm^3 of the solution was completely evaporated into the glass vacuum line and all mixtures were then manometrically made from the evaporated sample.

Results and Discussion

Fifty-eight experiments have been carried out to investigate the thermal decomposition of CH_3OH in the reflected shock wave regime over the *T*-range 1591−2865 K and reflected shock pressures between 0.3 and 1.1 atm. Four mixtures were used varying from 6.4 to 27.9 ppm CH_3OH diluted in Kr bath gas, and the conditions are given in Table 1. The temporal concentration buildup of OH was determined from measured absorbance, $(ABS)_t = \ln[I_0/I_t] = [OH]_t l \sigma_{OH}$, through an earlier determination[7] of the absorption cross-section at 308 nm ($\sigma_{OH} = (4.516-1.18 \times 10^{-3}T) \times 10^{-17}$ cm^2 $molecule^{-1}$ with $l =$ 489.7 cm). Typical results for two experiments are shown in Figure 1, where it is seen that the present sensitivity for OH-radical detection is significantly higher with 56 optical passes than in the previous work.[2,7,8]

As seen in Figure 1, the values for $[OH]_{max}$ show that more than one process is depleting CH_3OH because the levels of OH formed are always substantially less than $[CH_3OH]_0$. We find with constant $[CH_3OH]_0$ that relatively little OH is formed at low-*T* compared to high-*T*. Following the theoretical conclusions of Xia et al.[4] at high-*T*, only two dissociation processes are significant, reactions 1 and 2. In a companion paper (preceding article in this issue),[15] this conclusion is theoretically confirmed for the conditions of the present experiments. Hence, we include only reactions (1) and (2) in mechanistic fits.

TABLE 1: High-Temperature Rate Data for CH_3OH+ Kr → Products, OH+CH_3OH, and Values for the Branching Ratio.

P_1/Torr	M_s[a]	$\rho_5/(10^{18}$ $cm^{-3})$[b]	T_5/K[b]	k_1	k_3	α_1
		$X_{CH_3OH} = 2.390 \times 10^{-5}$				
10.94	2.777	2.271	1900	1.02(−15)[C]		0.78
10.95	2.879	2.349	2024	2.19(−15)		0.76
10.90	3.102	2.472	2328			0.79
10.93	2.940	2.382	2105	3.78(−15)		0.83
10.93	2.701	2.224	1799	2.47(−16)		0.65
10.92	2.575	2.129	1649	7.98(−17)	1.17(−11)	
10.94	2.581	2.137	1655	6.08(−17)	1.30(−11)	
10.98	2.577	2.142	1650	4.53(−17)	1.30(−11)	
10.92	2.802	2.291	1925	1.57(−15)		0.80
10.94	2.918	2.371	2076	3.20(−15)		0.77
10.90	2.626	2.164	1709	1.27(−16)	1.41(−11)	
10.94	2.647	2.187	1734	1.76(−16)		0.60
10.89	2.525	2.084	1591	4.22(−17)	1.26(−11)	
10.94	2.588	2.142	1663	6.54(−17)	1.32(−11)	
		$X_{CH_3OH} = 1.257 \times 10^{-5}$				
10.95	3.440	2.659	2832			0.76
10.93	3.424	2.647	2807			0.76
10.93	2.834	2.315	1966	1.73(−15)		0.75
10.98	3.283	2.589	2591			0.87
10.95	2.921	2.375	2079	3.37(−15)		0.75
10.93	2.838	2.318	1972	1.68(−15)		0.70
10.95	2.911	2.369	2067	2.74(−15)		0.72
10.92	3.013	2.425	2204	6.19(−15)		0.70
10.92	3.073	2.460	2287	1.14(−14)		0.73
10.89	2.876	2.334	2020	2.23(−15)		0.85
5.90	3.183	1.367	2466			0.77
5.92	3.258	1.393	2577			0.77
5.97	3.196	1.387	2485			0.70
5.91	3.444	1.441	2865			0.85
5.97	3.392	1.442	2783			0.80
5.93	3.165	1.368	2439			0.63
5.97	3.112	1.364	2359			0.76
5.96	2.987	1.324	2181	7.55(−15)		0.67
5.99	3.128	1.376	2378			0.77
5.91	3.084	1.342	2320			0.70
5.96	3.005	1.325	2213	8.23(−15)		0.64
5.98	3.001	1.329	2208	9.03(−15)		0.65
5.93	2.942	1.298	2127	6.61(−15)		0.65
15.99	2.666	3.193	1756	1.41(−16)		0.50
15.89	2.650	3.156	1738	9.34(−17)		0.50
15.98	2.751	3.279	1861	4.88(−16)		0.55
15.89	2.773	3.282	1888	7.92(−16)		0.50
		$X_{CH_3OH} = 2.793 \times 10^{-5}$				
5.94	3.269	1.411	2576			0.91
5.94	3.139	1.372	2385			0.85
5.94	3.139	1.372	2385			0.87
5.94	2.875	1.285	2024	2.02(−15)		0.70
5.96	2.819	1.270	1952	1.89(−15)		0.75
5.88	2.796	1.245	1923	1.00(−15)		0.78
5.93	2.623	1.188	1710	1.18(−16)	9.90(−12)	
5.96	2.669	1.213	1765	3.30(−16)		0.60
5.95	2.605	1.185	1688	2.39(−16)	1.37(−11)	
		$X_{CH_3OH} = 6.373 \times 10^{-6}$				
15.88	3.066	3.546	2278			0.83
15.98	2.838	3.364	1971	1.63(−15)		0.67
15.98	2.804	3.331	1928	1.55(−15)		0.68
15.92	2.904	3.413	2058	2.29(−15)		0.77
15.91	2.764	3.289	1872	7.30(−16)		0.80
15.87	3.017	3.514	2202	4.27(−15)		0.77
15.89	2.974	3.481	2143	4.31(−15)		0.75
15.86	3.107	3.588	2328			0.75

[a] The error in measuring the Mach number, M_s, is typically 0.5−1.0% at the one standard deviation level. [b] Quantities with the subscript 5 refer to the thermodynamic state of the gas in the reflected shock region. [c] Numbers in parentheses denotes the power of 10.

Results in the *T*-Range 2278−2865 K. Inspection of the high-*T* results in Figure 1 shows that formation rates are too

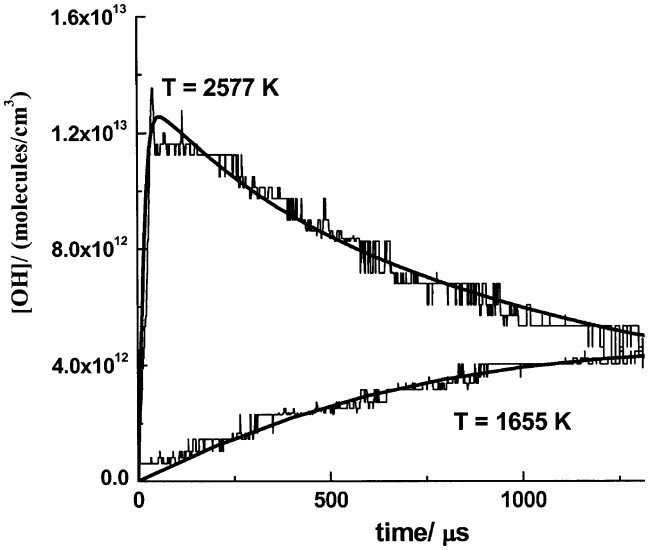

Figure 1. Two [OH] temporal profiles measured at high- and low-*T*. Solid lines: fits with the full reaction mechanism listed in Table 2 with optimized k_1 and/or α_1 and/or k_3 (see text). The conditions for the high-*T* profile are $P_1 = 5.92$ Torr and $M_s = 3.258$, $T_5 = 2577$ K, $\rho_5 = 1.393 \times 10^{18}$ molecules cm^{-3}, and $[CH_3OH]_0 = 1.752 \times 10^{13}$ molecules cm^{-3}. The low-*T* conditions are $P_1 = 10.94$ Torr and $M_s = 2.581$, $T_5 = 1655$ K, $\rho_5 = 2.137 \times 10^{18}$ molecules cm^{-3}, and $[CH_3OH]_0 = 5.109 \times 10^{13}$ molecules cm^{-3}.

fast to be time-resolved and, therefore, estimates of k_1 and k_2 are impossible. However, the branching ratio, $\alpha_1 = k_1/(k_1 + k_2) \cong [OH]_0/[CH_3OH]_0$ can be evaluated from these experiments because extrapolation to zero time is possible. Recognizing that the depletion of initially formed radicals, CH_3, OH, and $^3CH_2$, will involve second-order reactions following nearly instantaneous formation, we have estimated $[OH]_0$ simply by carrying out a second-order extrapolation to zero time, i.e., plotting $[[OH]_t]^{-1}$ against time. In the example shown, the extrapolated value determined for α_1 is ~0.8. This initial estimate is then used in chemical modeling fits based on the thirty-six step mechanism given in Table 2 (rate constants with references are listed in the table). For the dissociation experiments, only the first twenty-nine reactions are important. The sensitivity analysis shown in Figure 2 for the high-*T* experiment in Figure 1 indicates that second-order processes involving the products of the dissociation, namely, OH, CH_3, and $^3CH_2$, are important in the long-time depletion of [OH] over the 1.5 ms observation time.

Using the Table 2 mechanism, the solid line for the high-*T* experiment in Figure 1 is a fit with k_1 and α_1 as the fitting parameters to explain both the fast rise of [OH] and $[OH]_{max}$. For the $T >$ ~2300 K experiments, the values for the parameters were chosen to be compatible with the measured approximate branching ratio and $[OH]_{max}$ even though, as mentioned above, the k_1 values were not used in the dissociation rate constant analysis. To best fit the experiment shown in Figure 1, the modified value for α_1 was 0.77. Using the mechanism, the [OH] depletion profiles for all experiments above 2300 K were within <~5−10% of the measured profile, suggesting that the secondary depletion reaction rate constants involving OH are adequate, a conclusion that is discussed further below. Hence, branching ratios are the only quantities obtainable from the high-*T* experiments. These are listed in Table 1.

Results in the *T*-Range 1591−1710 K. For the 1655 K experiment shown in Figure 1 and other low-*T* experiments between 1591 and 1710 K listed in Table 1, sensitivity analysis shows that the only significant OH-radical depletion process is OH + CH_3OH (reaction 3 in Table 2); i.e., all radical−radical reactions contribute <5% to the profiles at long times. Hence, the fits depend on values for k_1 and k_3, thereby giving a method for determining both rate constants. The fitted values (k_1 and k_3) for these low-*T* experiments are listed in Table 1.

For OH + CH_3OH (k_3 in Table 2), previous evaluations[1] have been made. There are six direct experimental determinations[40−45] that are mostly in the lower-*T* regime, the most accurate being that of Hess and Tully.[43] At 1200 K, Bott and Cohen[46] report a value of 8.63×10^{-12} cm^3 molecule^{-1} s^{-1}. Using the Arrhenius and three-parameter equations that describe the results from these six studies,[40−45] a database has been constructed over equal intervals of T^{-1}. Six points from each of the six *T*-dependent studies are calculated from the equations, but only over the *T*-range of the individual studies. The single point from Bott and Cohen is also included. The lines and points from Bott and Cohen and also from Table 1 are plotted in Figure 3. Because the Hess and Tully determination is the most accurate, it was given double weight. Hence, these 43 points combined with the 8 points from Table 1 constitute the database for determining an evaluation from 210 to 1710 K. It should be noted that the present determination is the most direct to date in the higher-*T* regime. The database was then fitted to the modified Arrhenius equation, $k = AT^n \exp(-B/T)$, yielding

$$k_3 = 2.96 \times 10^{-16} T^{1.4434} \exp(-57\ \mathrm{K}/T)\ \mathrm{cm}^3\ \mathrm{molecule}^{-1}\ \mathrm{s}^{-1} \quad (7)$$

Equation 7 is shown as the thick solid line in Figure 3. The data of Hagele et al.[40] are within ±12%, those of Meier et al.[41] range from 7% higher to 18% lower, those of Greenhill and O'Grady[42] are 4% higher to 18% lower, those of Hess and Tully[43] range from 24% higher to 4% lower, those of Jimenez et al.[44] are from 1% higher to 7% lower, and those of Dillon et al.[45] are higher by 3−12%, than values calculated from eq 7. At 1200 K, eq 7 gives 7.8×10^{-12} cm^3 molecule^{-1} s^{-1}, in good agreement with the single point of Bott and Cohen. Hence, eq 7 is an excellent representation of the data used to obtain it, within experimental error, and is therefore listed in Table 2 as the preferred value for k_3.

Tsang has presented an experimental evaluation[47] that is in adequate agreement (±20%) with eq 7 up to ~1500 K; however, this evaluation diverges from (7) being about 2 times higher at 2800 K. There are two flame studies where k_3 is estimated from fits to complex mechanisms.[48,49] The inferences of Vandooren and Van Tiggelen[48] between 1000 and 2000 K are ~60% higher whereas those of Li and Williams[49] between 300 and 2500 K are 4−40% lower than (7). There are two theoretical investigations[50,51] both of which substantially overestimate k_3 particularly at high-*T*.

Results in the *T*-Range 1734−2287 K. For the intermediate temperature experiments, $[OH]_t$ at short times is dominated by k_1 and k_2 (i.e., α_1). An example at 1925 K is shown in Figure 4. However, as seen in Figure 5, sensitivity analysis shows that the significant depletion reactions are OH + CH_3OH, OH + OH, CH_3 + OH, and $^3CH_2$ + OH, with the relative importance depending on *T*. Equation 7 is used for OH + CH_3OH, but for OH + OH (k_{12} in Table 2), direct rate constants have been measured by Wooldridge et al.,[22] and these are consistent with O + $H_2O \rightarrow$ OH + OH (k_{13} in Table 2) transformed through equilibrium constants[9] using the recent re-evaluation for the heat of formation of OH radicals.[19,20] Hence, both of the self-combination reactions for OH and CH_3 radicals are characterized and are not varied in the simulations.

The most recent direct experimental measurement for the cross-combination reaction, CH_3 + OH reaction (k_4 in Table 2) at $T >$ 850 K, was performed in this laboratory.[2] Even though

TABLE 2: Mechanism for Fitting [OH] Profiles from the CH_3OH Dissociation[a]

1	$CH_3OH + Kr \rightarrow CH_3 + OH + Kr$	k_1 = to be fitted
2	$CH_3OH + Kr \rightarrow {}^1CH_2 + H_2O + Kr$	k_2 = to be fitted
3	$OH + CH_3OH \rightarrow H_2CO + H_2O + H$	$k_3 = 2.96 \times 10^{-16} T^{1.4434} \exp(-57\ K/T)$ (eq 7)
4	$CH_3 + OH \rightarrow {}^1CH_2 + H_2O$	$k_4 = 1.15 \times 10^{-9}\ T^{-0.4884}$ [2]
5	$CH_3 + O \rightarrow H_2 + CO + H$	$k_5 = 2.52 \times 10^{-11}$ [16, 17]
6	$H + O_2 \rightarrow OH + O$	$k_6 = 1.62 \times 10^{-10} \exp(-7474\ K/T)$ [18]
7	$OH + O \rightarrow O_2 + H$	$k_7 = 5.42 \times 10^{-13} T^{0.375} \exp(950\ K/T)$ [9, 19, 20]
8	$O + H_2 \rightarrow OH + H$	$k_8 = 8.44 \times 10^{-20} T^{2.67} \exp(-3167\ K/T)$ [9]
9	$OH + H \rightarrow H_2 + O$	$k_9 = 3.78 \times 10^{-20} T^{2.67} \exp(-2393\ K/T)$ [9, 19, 20]
10	$OH + H_2 \rightarrow H_2O + H$	$k_{10} = 3.56 \times 10^{-16} T^{1.52} \exp(-1736\ K/T)$ [21]
11	$H_2O + H \rightarrow OH + H_2$	$k_{11} = 1.56 \times 10^{-15} T^{1.52} \exp(-9083\ K/T)$ [9, 19, 20]
12	$OH + OH \rightarrow O + H_2O$	$k_{12} = 7.19 \times 10^{-21} T^{2.7} \exp(917\ K/T)$ [9, 19, 20, 22]
13	$O + H_2O \rightarrow OH + OH$	$k_{13} = 7.48 \times 10^{-20} T^{2.7} \exp(-7323\ K/T)$ [9, 19, 20]
14	$HCO + Kr \rightarrow H + CO + Kr$	$k_{14} = 6.00 \times 10^{-11} \exp(-7722\ K/T)$ [23]
15	$HO_2 + Kr \rightarrow H + O_2 + Kr$	$k_{15} = 7.614 \times 10^{-10} \exp(-22520\ K/T)$ [24]
16	$H_2CO + OH \rightarrow H_2O + HCO$	$k_{16} = 5.69 \times 10^{-15} T^{1.18} \exp(225\ K/T)$ [25]
17	$CH_3 + CH_3 \rightarrow C_2H_6$	$k_{17} = (\rho, T)$ [8]
18	$CH_3 + CH_3 \rightarrow C_2H_4 + 2H$	$k_{18} = 5.26 \times 10^{-11} \exp(-7392\ K/T)$ [26]
19	$CH_3 + O \rightarrow H_2CO + H$	$k_{19} = 1.148 \times 10^{-10}$ [16, 17]
20	$H_2CO + O \rightarrow OH + HCO$	$k_{20} = 6.92 \times 10^{-13} T^{0.57} \exp(-1390\ K/T)$ [25]
21	$OH + C_2H_4 \rightarrow H_2O + H + C_2H_2$	$k_{21} = 3.35 \times 10^{-11} \exp(-2990\ K/T)$ [27]
22	$^1CH_2 + Kr \rightarrow {}^3CH_2 + Kr$	$k_{22} = 4.0 \times 10^{-14} T^{0.93}$ [28, 29]
23.	$HO_2 + OH \rightarrow H_2O + O_2$	$k_{23} = 2.35 \times 10^{-10} T^{-0.21} \exp(56\ K/T)$ [30]
24	$H_2CO + Kr \rightarrow HCO + H + Kr$	$k_{24} = 1.019 \times 10^{-8} \exp(-38706\ K/T)$ [31]
25	$H_2CO + Kr \rightarrow H_2 + CO + Kr$	$k_{25} = 4.658 \times 10^{-9} \exp(-32110\ K/T)$ [31]
26	$OH + {}^3CH_2 \rightarrow CH_2O + H$	$k_{26} = 1.110 \times 10^{-10} T^{0.0166} \exp(-9.1\ K/T)$ [32]
27	$^3CH_2 + {}^3CH_2 \rightarrow C_2H_2 + 2H$	$k_{27} = 2.395 \times 10^{-10} T^{0.0254} \exp(-17.1\ K/T)$ [32]
28	$^3CH_2 + CH_3 \rightarrow C_2H_4 + H$	$k_{28} = 1.894 \times 10^{-10} T^{-0.1317} \exp(-8.2\ K/T)$ [32]
29	$^3CH_2 + H \rightarrow CH + H_2$	$k_{29} = 2 \times 10^{-10}$ [32]
30	$CH_3I + Kr \rightarrow CH_3 + I + Kr$	$k_{30} = 8.04 \times 10^{-9} \exp(-20566\ K/T)$ [33]
31	$O + C_2H_6 \rightarrow OH + H + C_2H_4$	$k_{31} = 1.87 \times 10^{-10} \exp(-3950\ K/T)$ [34]
32	$C_4H_{10}O_2 \rightarrow OH + CH_3 + (CH_3)_2CO$	$k_{32} = 2.5 \times 10^{15} \exp(-21649\ K/T)$ [35]
33	$OH + CH_3I \rightarrow H_2O + CH_2I$	$k_{33} = 2.72 \times 10^{-24} T^{3.97} \exp(447\ K/T)$ [36]
34	$OH + (CH_3)_2CO \rightarrow H_2O + CH_2COCH_3$	$k_{34} = 4.90 \times 10^{-11} \exp(-2297\ K/T)$ [37]
35	$OH + C_2H_6 \rightarrow H_2O + H + C_2H_4$	$k_{35} = 2.68 \times 10^{-18} T^{2.22} \exp(-373\ K/T)$ [38]
36	$C_2H_6 \rightarrow 2CH_3$	$k_{36} = k_{17}/(1.4058 \times 10^{27} \exp(-44521\ K/T))$ [39]

[a] All rate constants are in cm^3 molecule^{-1} s^{-1} except for reaction 32, which is in s^{-1}. Numbers in brackets are reference numbers.

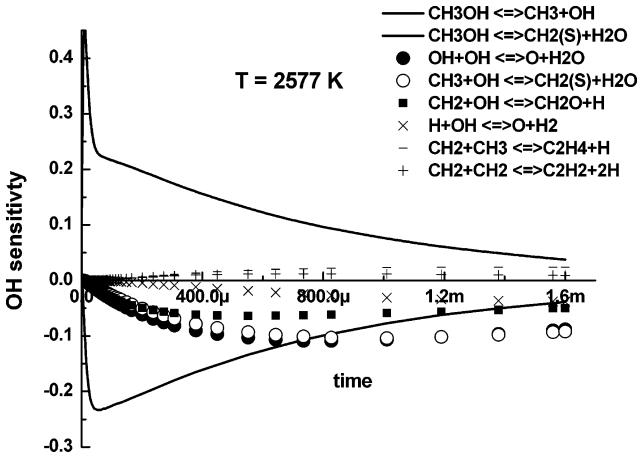

Figure 2. OH-radical sensitivity analysis for the 2577 K profile shown in Figure 1 using the full reaction mechanism scheme and the final fitted value for α_1 listed in Table 1. The eight most sensitive reactions are shown.

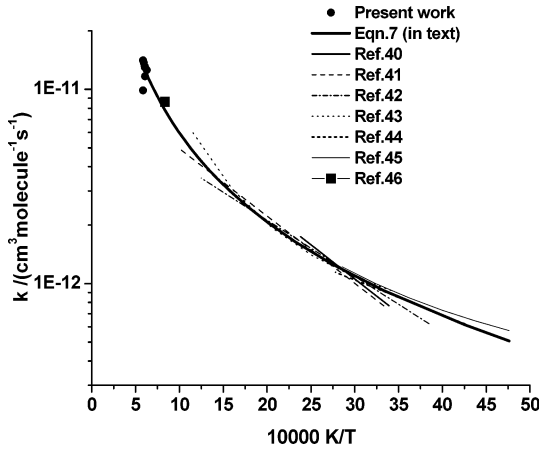

Figure 3. Arrhenius plot of the data (●) for k_3 from Table 1 (1591−1710 K). The solid thick line is calculated from the present evaluation (see text and eq 7) based on the present values and refs 40−46.

the values reported for k_4 (and the derived least-squares expression for 200−2400 K; i.e., $k_4 = 1.15 \times 10^{-9} T^{-0.4884}$ cm^3 molecule^{-1} s^{-1}) agree well with the lower-T experiments and theory of De A. Pereira et al.,[52] theoretical estimates from the preceding paper,[15] that include both the singlet and triplet potential energy pathways,[53] cast doubt on this result, particularly in the ∼850−1150 K temperature range where tBH and di-*tert*-butyl peroxide were used as sources of OH and CH_3 radicals. The earlier data along with the least-squares correlation[2] and new theoretical calculations are shown in Figure 6 where it is seen that the earlier values in the 1734−2287 K range, obtained using CH_3OH/CH_3I mixtures, agrees well with the new theory. This is only possible if the triplet pathway is included as pointed out in the earlier work.[2]

There is, however, a substantial disagreement in the lower-T region, and this has prompted new experiments using both tBH and tBH/CH_3I mixtures. The conditions of these experiments, obtained with 36 optical passes, are given in Table 3. Figure 7 is a typical result at 1226 K. In all experiments, the fitted values for $[tBH]_0$ (column 6 in Table 3) that reproduced the OH profiles were in excellent agreement with a priori estimates based on the initial assay of the tBH solution (i.e., 32 mol % tBH) and subsequent mole fractions of mixtures deduced from Baratron

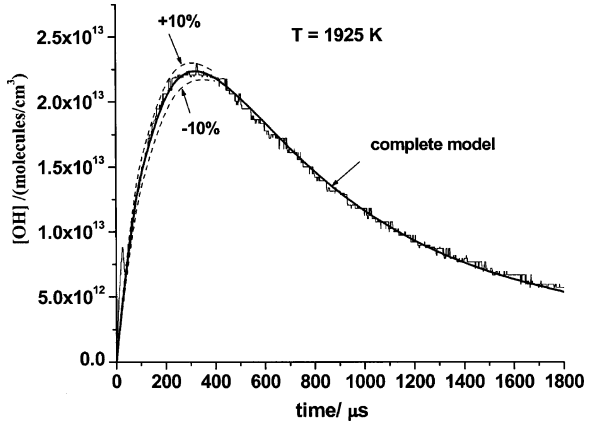

Figure 4. [OH] temporal profile measured at intermediate-*T*. Solid line: fit with the full reaction mechanism listed in Table 2 with optimized k_1 and α_1. Dashed lines: fits with k_1 and k_2 varied by ±10%. The conditions for this profile are $P_1 = 10.92$ Torr, $M_s = 2.802$, $T_5 = 1925$ K, $\rho_5 = 2.291 \times 10^{18}$ molecules cm^{-3}, and $[CH_3OH]_0 = 5.475 \times 10^{13}$ molecules cm^{-3}.

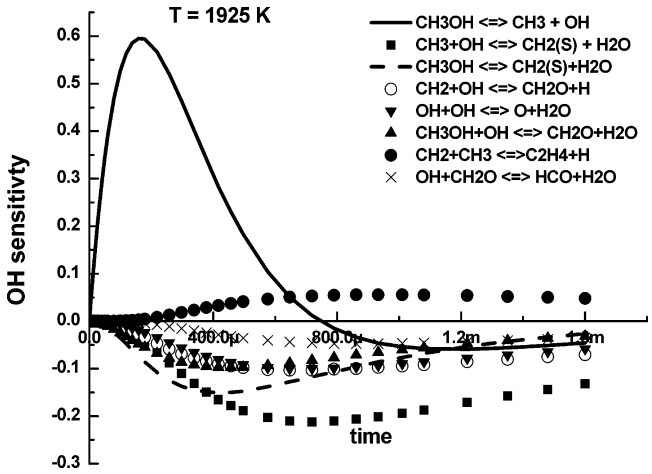

Figure 5. OH-radical sensitivity analysis for the 1925 K profile shown in Figure 4 using the full reaction mechanism scheme and the final fitted values for k_1 and α_1 listed in Table 1. The eight most sensitive reactions are shown.

pressure measurements. There is therefore good consistency between inferred $[OH]_t$ from the measured absorption cross section[7] and the tBH mole percent showing that no concentration is lost either in storage in the glass vacuum line or in transfer to the shock tube.

The [OH] sensitivity analysis corresponding to the profile in Figure 7 is shown in Figure 8. $[OH]_t$ is sensitive to the six reactions indicated in the figure with the $CH_3 + OH$ reaction contributing most to the profile. The known reaction, $OH + OH$,[22] also shows sensitivity at about the same level as $OH + (CH_3)_2CO$, reaction 34 in Table 2. In our earlier study,[2] this latter reaction was also included but was extrapolated from lower-*T* work.[54] The new 882−1300 K study by Vasudevan et al.[37] gives values between 7.0×10^{-12} and 8.4×10^{-12} cm^3 molecule^{-1} s^{-1} for the limited *T*-range, 1178−1299 K. Over this latter *T*-range, we performed five experiments with added acetone (not shown) and obtained $(7.3 \pm 0.7) \times 10^{-12}$ cm^3 molecule^{-1} s^{-1}, confirming the Vasudevan et al. result. The value extrapolated from the low-*T* work[54] is ∼5 times smaller than the new value, and this half an order of magnitude discrepancy is an important reason for the overestimation in the rate constants for $CH_3 + OH$ in the earlier study.[2]

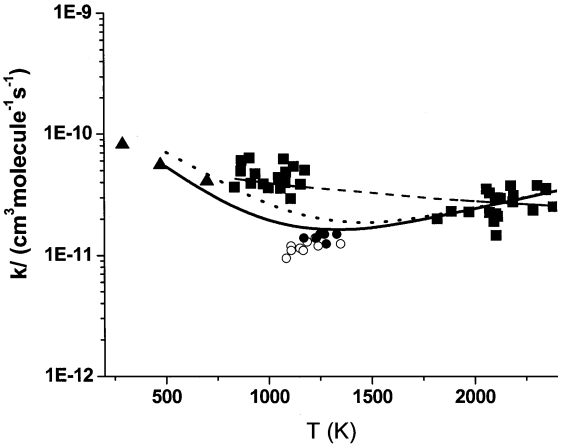

Figure 6. Rate coefficients for the $CH_3 + OH$ reaction: [●] ∼250 Torr; [○] ∼700 Torr (see Table 3). The thick solid line and dotted lines are recent theoretical calculations for 200 and 760 Torr, respectively, from ref 15. Key: [■] ref 2; dashed line ref 2 (see text); [▲] ref 52.

The $OH + {}^3CH_2$ reaction (k_{26} in Table 2) is the final reaction to consider in the intermediate temperature simulations. Regarding this reaction, CH_3OH and ketene (CH_2CO) were used as sources for OH and ${}^3CH_2$, respectively, yielding the only experimental measurement, $(2.6 \pm 1.6) \times 10^{-11}$ cm^3 molecule^{-1} s^{-1}, to date,[2] over the limited *T*-range 1887−2164 K. This value agreed well with the Tsang and Hampson recommendation[55] of 3.0×10^{-11} cm^3 molecule^{-1} s^{-1}. If this value is used in the complete mechanism, $[OH]_t$ is not well described in either the CH_3OH dissociation or the $CH_3 + OH$ experiments. Theoretical estimates[32] of this rate constant suggest values about 5 times larger, but use of this higher value by itself results in too much attenuation at longer times in both experiments. Therefore, rate constants between ${}^3CH_2$ and the other principal radicals have been added to the mechanism. These include ${}^3CH_2 + {}^3CH_2$, ${}^3CH_2 + CH_3$, and ${}^3CH_2 + H$ (reactions 27−29 in Table 2), and the rate constant values are taken from theoretical calculations[32] that utilize methodologies expected to have similar accuracies as the companion study.[15]

With these additions, the fits for the $CH_3 + OH$ profiles, like that shown in Figure 7, are well within ±5% of the data. The newly derived values for k_4 are listed in Table 3 and are plotted in Figure 6 along with the earlier data[2] and the new theoretical results.[15] Pressure dependence is predicted from theory, and this is only slightly indicated in the experimental data. The grand average of the values listed in the table give $(1.3 \pm 0.2) \times 10^{-11}$, to be compared to 1.65×10^{-11} cm^3 molecule^{-1} s^{-1} from theory, indicating good agreement in the ∼1100−1300 K temperature region in contrast to the earlier work.[2] The important point to note is that the least-squares correlation in the high-*T* region from the earlier work[2] is in excellent agreement with theory and is therefore used in the Table 2 mechanism.

For the CH_3OH dissociation experiments (Table 1) in both the intermediate- and high-*T* experiments (Figures 4 and 1), the description of OH depletion at long times requires a balance between $OH + CH_3$, reaction 4, and reactions 26−29 (all in Table 2). As stated above, we have elected to use theoretical values[32] for (26)−(29). It is important to stress that direct experimental confirmation of the theoretical values proposed for these reactions should be the subject of future research.

All the self- and cross-combination depletion reactions of OH, CH_3, and ${}^3CH_2$ radicals are now specified and are not varied in

TABLE 3: High-Temperature Rate Data for CH_3 + OH Reaction

P_1/Torr	M_s[a]	$\rho_5/(10^{18}$ cm$^{-3})$[b]	T_5/K[b]	k_4[c]	[tBH]/[tBH + H_2O]$_0$
		$X_{tBH+H_2O} = 4.188 \times 10^{-5}$			
10.93	2.215	1.863	1240	1.20(−11)[d]	0.33
10.95	2.166	1.824	1187	1.30(−11)	0.33
10.98	2.130	1.791	1151	1.15(−11)	0.33
10.93	2.060	1.709	1085	9.50(−12)	0.34
10.94	2.148	1.807	1168	1.10(−11)	0.34
10.99	2.085	1.745	1108	1.20(−11)	0.33
10.91	2.088	1.739	1109	1.10(−11)	0.33
10.99	2.205	1.870	1226	1.40(−11)	0.33
10.91	2.208	1.863	1226	1.40(−11)	0.33
10.97	2.325	1.982	1348	1.25(−11)	0.34
$X_{CH_3I} = 4.262 \times 10^{-5}$			$X_{tBH+H_2O} = 1.636 \times 10^{-5}$		
30.69	2.262	5.257	1271	1.50(−11)	0.29
30.60	2.243	5.211	1248	1.50(−11)	0.28
$X_{CH_3I} = 2.697 \times 10^{-5}$			$X_{tBH+H_2O} = 1.594 \times 10^{-5}$		
30.86	2.272	5.320	1278	1.25(−11)	0.28
30.80	2.168	5.060	1170	1.40(−11)	0.27
30.64	2.223	5.147	1232	1.40(−11)	0.27
30.72	2.321	5.411	1331	1.50(−11)	0.25

[a] The error in measuring the Mach number, M_s, is typically 0.5−1.0% at the one standard deviation level. [b] Quantities with the subscript 5 refer to the thermodynamic state of the gas in the reflected shock region. [c] Rate constants in units cm^3 molecule^{-1} s^{-1}. [d] Parentheses denotes the power of 10.

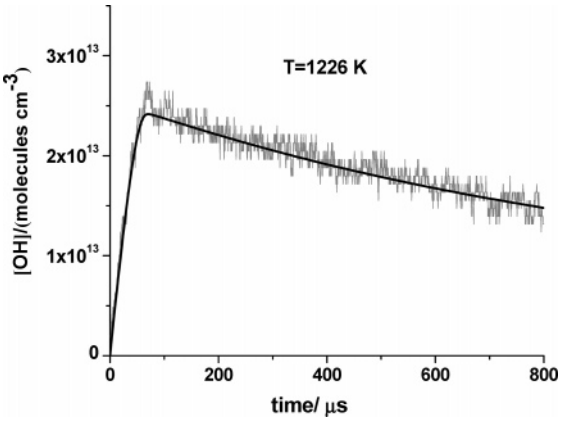

Figure 7. Sample temporal profile of OH absorption at low-T using tBH, $(CH_3)_3COOH$, as the source for OH radicals. Solid line: fit using the reaction mechanism of Table 2. The experimental conditions are P_1 = 10.99 Torr, M_s = 2.205, T_5 = 1226 K, $\rho_5 = 1.870 \times 10^{18}$ molecules cm^{-3}, and [tBH]$_0 = 2.550 \times 10^{13}$ molecules cm^{-3}.

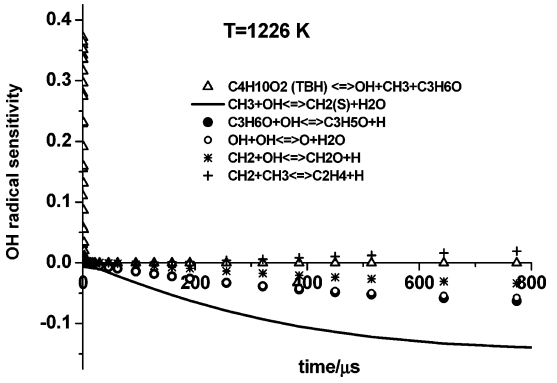

Figure 8. OH-radical sensitivity analysis for the profile shown in Figure 7 using the full reaction mechanism scheme and the final fitted values of $k_4 = 1.4 \times 10^{-11}$ cm^3 molecule^{-1} s^{-1}. The six most sensitive reactions are shown.

the simulations. The fits are then carried out by only varying dissociation rate constants. We found that all high- and intermediate-T experiments can be fitted to within <∼5−10% over the entire time range with the proposed mechanism. As

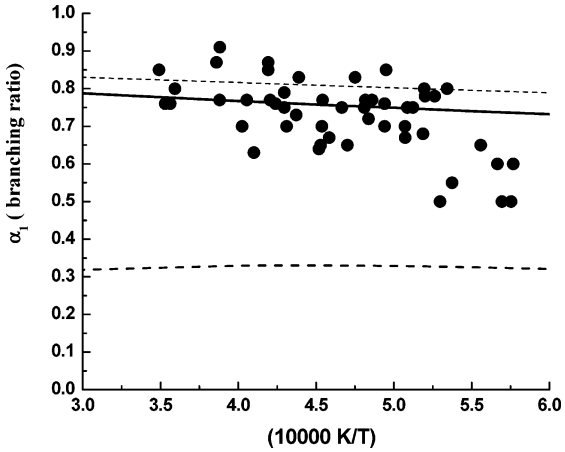

Figure 9. Branching ratios, α_1, from Table 1 plotted against T^{-1}. [●] Present work with an average value between 1734 and 2865 $K = 0.73 \pm 0.09$. The thin dashed line (760 Torr) and thick solid line (200 Torr) are theoretical calculations from ref 15 and the thick dashed line is from ref 4.

stated above, the high-T experiments yield only α_1 values, but initial time resolution in the intermediate-T range allows for estimates of both k_1 and k_2 and, therefore, α_1.

Fortunately in the intermediate-T regime, as seen in Figures 4 and 5, the initial profiles are mostly sensitive to CH_3OH dissociation rates. At T = 1925 K, uncertainties of ±10% in both k_1 and k_2 for constant α_1 result in fits that are either too low or too high as shown in Figure 4 by the dashed lines. The simulation using the complete mechanism is also shown in the figure with the final fitted values for k_1 and α_1. These values for the intermediate temperature regime experiments are listed in Table 1. As stated previously, these values give good profiles, suggesting that the OH, CH_3, and $^3CH_2$ depletion reaction rate constants are supplying excellent descriptions of all experiments.

The α_1 determinations are plotted against T^{-1} in Figure 9, and even though there is substantial data scatter, a slight T-dependence is suggested. This is further illustrated in Figure 10 where Arrhenius plots of the k_1 and k_2 values calculated from

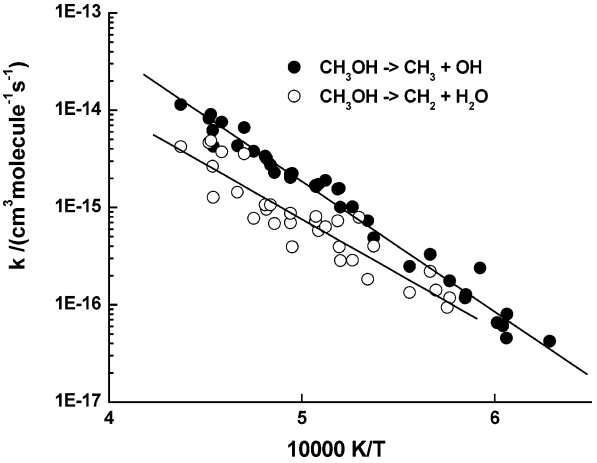

Figure 10. Arrhenius plot of the data, (●) and (○), for k_1 and k_2, respectively, from Table 1. The lines are calculated from eqs 8 and 9, respectively.

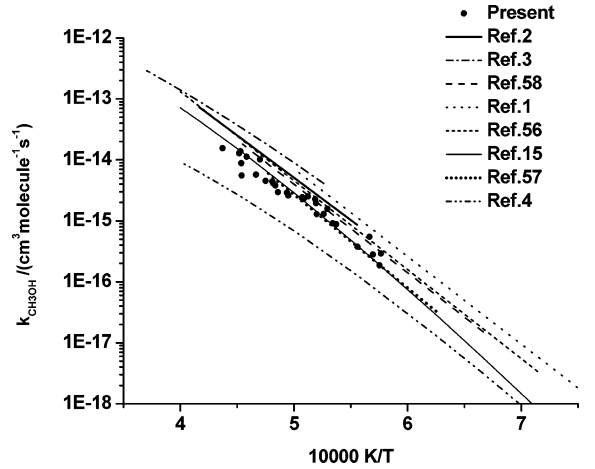

Figure 11. Arrhenius plot of the data for $k_{total} = k_1 + k_2$ from Table 1 shown as [●]. The lines noted in the inset are from refs 1−4, 15, and 56−58.

α_1 are shown along with linear-least-squares analyses that include all of the points in Table 1. The analyses give

$$\ln k_1 = -(18.49 \pm 0.45) - (30857 \pm 855\ \mathrm{K})/T \quad (8)$$

and

$$\ln k_2 = -(21.84 \pm 0.98) - (25946 \pm 1935\ \mathrm{K})/T \quad (9)$$

where the rate constants have units, cm^3 molecule^{-1} s^{-1}. The points in Table 1 are within ±32 and ±48% at one standard deviation of the lines determined from eqs 8 and 9, respectively. Summing the values for k_1 and k_2 for each experiment in Table 1 gives k_{total} as a function of temperature, and these points are shown in Figure 11. Linear-least-squares analysis over the T-range 1734−2287 K yields

$$\ln k_{total} = -(18.98 \pm 0.59) - (29171 \pm 1165\ \mathrm{K})/T \quad (10)$$

The summed points are within ±26% of eq 10 at the one standard deviation level.

There are several earlier studies on the thermal decomposition of CH_3OH,[1] and rate constants vary by about a factor of 40 over the present temperature range. The present result for k_{total}, summarized by eq 10, is about one-half of the earlier determination from this laboratory[2] and is therefore slightly outside the combined experimental error of the present and earlier study. The k_{total} results of Cribb et al.[3] are about three times higher than eq 10. The 2005 Baulch et al. evaluation[1] suggests values 1.6−2.5 times higher than the present value. The more recent results by Koike et al.[56] between 1400 and 2400 K give k_{total} values that agree with eq 10 up to ∼1750 K but then diverge to 2.5 times the present value at 2400 K. There are two studies from Wagner and co-workers.[57,58] The Spindler and Wagner results[57] range from 0.4 to 1.2 of eq 10 over their T-range, 1600−2200 K and therefore agree best with the present work whereas the experimental results of Dombrowsky et al.[58] give values that agree well with the present work from 1600 to 1800 K but then diverge to 1.8 times larger at 2200 K. These comparisons are shown graphically in Figure 11 along with the theoretical value for k_{total} from the preceding paper.[15] The earlier theoretical results by Xia et al.[4] are also shown in the figure where the overall rate constant appears to be underestimated by a nearly a factor of 10. In the earlier work from this laboratory,[2] the only process considered to be important was reaction 1. The measured branching ratios in the present work shown in Figure 9 disagree with this conclusion and with the theoretical conclusions of Xia et al.[4] but agree well with the results of Dombrowsky et al.[58] The new theory[15] is in good agreement with the data even though the scatter precludes observing the predicted pressure dependence.

In conclusion, the reflected shock tube technique with multipass absorption spectrometric detection of $[OH]_t$ has been used to study the dissociation of methanol between 1591 and 2865 K. Rate constants for two product channels, (1) CH_3 + OH and (2) $^1CH_2 + H_2O$, were determined.

$$k_1 = 9.33 \times 10^{-9} \exp(-30857\ \mathrm{K}/T) \text{ for } 1591-2287\ \mathrm{K}$$

$$k_2 = 3.27 \times 10^{-10} \exp(-25946\ \mathrm{K}/T) \text{ for } 1734-2287\ \mathrm{K}$$

Several other rate processes contributed to the profile fits, and rate constants for $OH + CH_3OH \rightarrow$ products, $OH + (CH_3)_2CO \rightarrow CH_2COCH_3 + H_2O$, and $OH + CH_3 \rightarrow {}^{1,3}CH_2 + H_2O$, were subsequently determined as

$$k_{OH+CH_3OH} = 2.96 \times 10^{-16} T^{1.4434} \exp(-57\ \mathrm{K}/T) \text{ for } 210-1710\ \mathrm{K}$$

$$k_{OH+(CH_3)_2CO} = (7.3 \pm 0.7) \times 10^{-12} \text{ for } 1178-1299\ \mathrm{K}$$

$$k_{OH+CH_3} = (1.3 \pm 0.2) \times 10^{-11} \text{ for } 1000-1200\ \mathrm{K}$$

All are in cm^3 molecule^{-1} s^{-1}. The measured branching ratio is ∼0.8 between reactions 1 and 2. In the preceding article in this issue,[15] a theoretical analysis of the dissociation is presented along with a theoretical analysis for the OH + CH_3 reaction. The comparison of theory to experiment both with regard to the branching ratio and absolute values for both reactions is excellent as is specifically shown in Figures 6, 9, and 11.

Acknowledgment. We thank Drs. Jasper, Klippenstein, and Harding for supplying us with their theoretical results prior to publication. This work was supported by the U.S. Department of Energy, Office of Basic Energy Sciences, Division of Chemical Sciences, Geosciences and Biosciences under Contract No. DE-AC02-06CH11357.

References and Notes

(1) (a) *NIST Chemical Kinetics Database*; NIST Standard Reference Database 17; Gaithersburg, MD, 2000. (b) Baulch, D. L.; Bowman, C. T.;

Cobos, C. J.; Cox, R. A.; Just, Th.; Kerr, J. A.; Pilling, M. J.; Stocker, D.; Troe, J.; Tsang, W.; Walker, R. W.; Warnatz, J. *J. Phys. Chem. Ref. Data* **2005**, *34*, 1059.

(2) Krasnoperov, L. N.; Michael, J. V. *J. Phys. Chem. A* **2004**, *108*, 8317.

(3) Cribb, P. H.; Dove, J. E.; Yamazaki, S. *Combust. Flame* **1992**, *88*, 169.

(4) Xia, W. S.; Zhu, R. S.; Lin, M. C.; Mebel, A. M. *Faraday Discuss.* **2001**, *119*, 19.

(5) Su, M.-C.; Kumaran, S. S.; Lim, K. P.; Michael, J. V. *Rev. Sci. Instrum.* **1995**, *66*, 4649.

(6) Su, M.-C.; Kumaran, S. S.; Lim, K. P.; Michael, J. V.; Wagner, A. F.; Harding, L. B.; Fang, D.-C. *J. Phys. Chem. A* **2002**, *106*, 8261.

(7) Srinivasan, N. K.; Su, M.-C.; Sutherland, J. W.; Michael, J. V. *J. Phys. Chem. A* **2005**, *109*, 1857.

(8) Srinivasan, N. K.; Su, M.-C.; Sutherland, J. W.; Michael, J. V. *J. Phys. Chem. A* **2005**, *109*, 7902.

(9) Michael, J. V. *Prog. Energy Combust. Sci.* **1992**, *18*, 327.

(10) Michael, J. V. In *Advances in Chemical Kinetics and Dynamics*; Barker, J. R., Ed.; JAI: Greenwich, 1992; Vol. I, pp 47−112, for original references.

(11) Michael, J. V.; Sutherland, J. W. *Int. J. Chem. Kinet.* **1986**, *18*, 409.

(12) Michael, J. V. *J. Chem. Phys.* **1989**, *90*, 189.

(13) Michael, J. V.; Fisher, J. R. In *Seventeenth International Symposium on Shock Waves and Shock Tubes*; Kim, Y. W., Ed.; AIP Conference Proceedings 208; American Institute of Physics: New York, 1990; pp 210−215.

(14) Su, M.-C.; Kumaran, S. S.; Lim, K. P.; Michael, J. V.; Wagner, A. F.; Dixon, D. A.; Kiefer, J. H.; DiFelice, J. *J. Phys. Chem.* **1996**, *100*, 15827.

(15) Jasper, A. W.; Klippenstein, S. J.; Harding, L. B. *J. Phys. Chem. A*, **2007**, *111*, 3932.

(16) Lim, K. P.; Michael, J. V. *J. Chem. Phys.* **1993**, *98*, 3919.

(17) Fockenberg, C.; Hall, G. E.; Preses, J. M.; Sears, T. J.; Muckerman, J. T. *J. Phys. Chem. A* **1999**, *103*, 5722. Preses, J. M.; Fockenberg, C.; Flynn, G. W. *J. Phys. Chem. A* **2000**, *104*, 6758.

(18) Du, H.; Hessler, J. P. *J. Chem. Phys.* **1992**, *96*, 1077.

(19) Ruscic, B.; Wagner, A. F.; Harding, L. B.; Asher, R. L.; Feller, D.; Dixon, D. A.; Peterson, K. A.; Song, Y.; Qian, X.; Ng, C. Y.; Liu, J.; Chen, W.; Schwenke, D. W. *J. Phys. Chem. A* **2002**, *106*, 2727.

(20) Herbon, J. T.; Hanson, R. K.; Golden, D. M.; Bowman, C. T. *Proc. Combust. Inst.* **2002**, *29*, 1201.

(21) Oldenborg, R. C.; Loge, G. W.; Harridine, D. M.; Winn, K. R. *J. Phys. Chem.* **1992**, *96*, 8426.

(22) Wooldridge, M. S.; Hanson, R. K.; Bowman, C. T. *Int. J. Chem. Kinet.* **1994**, *26*, 389.

(23) Krasnoperov, L. N.; Chesnokov, E. N.; Stark, H.; Ravishankara, A. R. *J. Phys. Chem. A* **2004**, *108*, 11526.

(24) Michael, J. V.; Su, M.-C.; Sutherland, J. W.; Carroll, J. J.; Wagner, A. F. *J. Phys. Chem. A* **2002**, *106*, 5297.

(25) Baulch, D. L.; Cobos, C. J.; Cox, R. A.; Esser, C.; Frank, P.; Just, Th.; Kerr, J. A.; Pilling, M. J.; Troe, J.; Walker, R. W.; Warnatz, J. *J. Phys. Chem. Ref. Data* **1992**, *21*, 411.

(26) Lim, K. P.; Michael, J. V. *Proc. Combust. Inst.* **1994**, *25*, 713.

(27) Tully, F. P. *Chem. Phys. Lett.* **1988**, *143*, 510.

(28) Langford, A. O.; Petek, H.; Moore, C. B. *J. Chem. Phys.* **1983**, *78*, 6650.

(29) Hancock, G.; Heal, M. R. *J. Phys. Chem.* **1992**, *96*, 10316.

(30) Gonzalez, C.; Theisen, J.; Schlegel, H. B.; Hase, W. L.; Kaiser, E. W. *J. Phys. Chem.* **1992**, *96*, 1767.

(31) Kumaran, S. S.; Carroll, J. J.; Michael, J. V. *Proc. Combust. Inst.* **1998**, *27*, 125.

(32) Jasper, A. W.; Klippenstein, S. J.; Harding, L. B. Private communication, Oct 2006.

(33) Kumaran, S. S.; Su, M.-C.; Michael, J. V. *Int. J. Chem. Kinet.* **1997**, *29*, 535.

(34) Michael, J. V.; Keil, D. G.; Klemm, R. B. *Int. J. Chem. Kinet.* **1985**, *15*, 705.

(35) Vasudevan, V.; Davidson, D. F.; Hanson, R. K. *Int. J. Chem. Kinet.* **2005**, *37*, 98.

(36) Marshall, P.; Misra, A.; Berry, R. J. *Chem. Phys. Lett.* **1997**, *265*, 48.

(37) Vasudevan, V.; Davidson, D. F.; Hanson, R. K. *J. Phys. Chem. A* **2005**, *109*, 3352.

(38) Krasnoperov, L. N.; Michael, J. V. *J. Phys. Chem. A* **2004**, *108*, 5643.

(39) Ruscic, B. Private communication of unpublished results obtained from Active Thermochemical Tables 1.25 and the Core (Argonne) Thermochemical Network 1.049 (2005) Tables.

(40) Hagele, J.; Lorenz, K.; Rhasa, D.; Zellner, R. *Ber. Bunsen-Ges. Phys. Chem.* **1983**, *87*, 1023.

(41) Meier, U.; Grotheer, H.-H.; Riekert, G.; Just. Th. *Ber. Bunsen-Ges. Phys. Chem.* **1985**, *89*, 325.

(42) Greenhill, P. G.; O'Grady, B. V. *Aust. J. Chem.* **1986**, *39*, 1775.

(43) Hess, W. P.; Tully, F. P. *J. Phys.Chem.* **1989**, *93*, 1944.

(44) Jimenez, E.; Gilles, M. K.; Ravishankara, A. R. *J. Photochem. Photobiol. A: Chem.* **2003**, *157*, 237.

(45) Dillon, T. J.; Hölscher, D.; Sivakumaran, V.; Horowitz, A.; Crowley, J. N. *Phys. Chem. Chem. Phys.* **2005**, *7*, 349.

(46) Bott, J. G.; Cohen, N. *Int. J. Chem. Kinet.* **1991**, *23*, 1075.

(47) Tsang, W. *J. Phys. Chem. Ref. Data* **1987**, *16*, 471.

(48) Vandooren, J.; Van Tiggelen, P. J. *Proc. Combust. Inst.* **1981**, *18*, 473.

(49) Li, S. C.; Williams, F. A. *Proc. Combust. Inst.* **1996**, *26*, 1017.

(50) Jodkowski, J. T.; Rayez, M.-T.; Rayez, J.-C. *J. Phys. Chem. A* **1999**, *103*, 3750.

(51) Xu, S.; Lin, M.-C. *Proc. Combust. Inst.*, in press.

(52) De A. Pereira, R.; Baulch, D. L.; Pilling, M. J.; Robertson, S. H.; Zeng, G. *J. Phys. Chem. A* **1997**, *101*, 9681.

(53) Wilson, C.; Balint-Kurti, G. G. *J. Phys. Chem. A* **1998**, *102*, 1625.

(54) Atkinson, R.; Baulch, D. L.; Cox, R. A.; Hampson, R. F., Jr.; Kerr, J. A.; Rossi, M. J.; Troe, J. *J. Phys. Chem. Ref. Data* **1997**, *26*, 521.

(55) Tsang. W.; Hampson, R. F. *J. Phys. Chem. Ref. Data* **1986**, *15*, 1087.

(56) Koike, T.; Kudo, M.; Maeda, I.; Yamada, H. *Int. J. Chem. Kinet.* **2000**, *32*, 1.

(57) Spindler, K.; Wagner, H. Gg. *Ber. Bunsen-Ges. Phys. Chem.* **1982**, *86*, 2.

(58) Dombrowsky, Ch.; Hoffman, A.; Klatt, M.; Wagner, H. Gg. *Ber. Bunsen-Ges. Phys. Chem.* **1991**, *95*, 1685.